17th World Conference on Earthquake Engineering, 17WCEE
Sendai, Japan - September 13th to 18th 2020

3D DYNAMIC EFFECTIVE STRESS ANALYSIS OF SOIL-PILE-STRUCTURE SYSTEMS IN NON-LIQUEFIED AND LIQUEFIED GROUND

Y. Nakagama[(1)], Y. Tamari[(2)], H. Yoshida[(3)] , M. Yamamoto[(4)] , H. Suzuki[(5)]

[(1)] *Bachelor, Tokyo Electric Power Services Co., Ltd., Tokyo, Japan, y.nakagama@tepsco.co.jp*
[(2)] *Doctor, Tokyo Electric Power Services Co., Ltd., Tokyo, Japan, etamari@tepsco.co.jp*
[(3)] *Doctor, Tokyo Electric Power Services Co., Ltd., Tokyo, Japan, yoshida@tepsco.co.jp*
[(4)] *Master, Tokyo Electric Power Services Co., Ltd., Tokyo, Japan, minoru-yamamoto@tepsco.co.jp*
[(5)] *Professor, Chiba Institute of Technology, Chiba, Japan, hiroko.suzuki@it-chiba.ac.jp*

Abstract

We conducted three-dimensional (3D) dynamic effective stress analysis of soil-pile-structure systems to validate the 3D finite element method (FEM) model used in practical seismic analysis. A pile foundation with 4 × 4 pile grouping and 2.5-diameter spacing was installed in both dry sand and liquefiable saturated sand. The two models were shaken in the horizontal direction under a centrifugal gravity of 30g. The 3D FEM model is used for dynamic analysis in which soils are simulated by a strain-space multiple-mechanism model, piles and super structure by shell elements, and the pile cap by eight-node brick elements. The calculated acceleration responses at the foundation top are consistent with measured accelerations for both non-liquefied and liquefied ground models. The calculated bending moments and shear forces at the pile tops are also in reasonable agreement with measured responses. The 3D FEM model with a strain-space multiple-mechanism model is therefore applicable to soil-pile-structure systems in liquefied ground to evaluate the dynamic behavior of systems subjected to horizontal motion.

Keywords: Soil-pile-structure system, Liquefied ground, Three-dimensional dynamic effective stress analysis

1. Introduction

Dynamic effective stress analysis is frequently used in performance-based design of pile foundations to evaluate structural response while considering dynamic interaction (e.g. [1]). Two-dimensional (2D) effective stress analysis is commonly used to consider interactions between piles and liquefied soil using simplified methods (e.g. [2]), whereas high-performance computing has recently allowed three-dimensional (3D) effective stress analysis of full-scale models. Although previous studies have endeavored to validate 3D analysis for dynamic interaction between pile and liquefiable soil [3][4][5], 3D effective stress analysis of pile foundations is rarely used in practical design likely owing to an insufficient number of validation cases.

In this study, we performed 3D dynamic effective stress analysis of shaking table tests of soil-foundation-structure systems to investigate the validity of this method for seismic responses. Non-liquefiable and liquefiable soil-pile-structure systems of 4 × 4 piles were examined from a series of existing shaking table tests [6].

2. Experimental procedure

We performed numerical simulations of shaking table tests of soil-foundation-structure systems at a centrifugal acceleration of 30g. We considered non-liquefiable soil-pile-structure systems (hereinafter referred to as dry sand model) and liquefiable soil-pile-structure systems (hereinafter referred to as saturated sand model), both using 4 × 4 piles. Fig. 1 shows the soil-pile-structure systems in the dry sand and saturated sand models. The geometric ratio between the model and prototype scales is 1:30 at a centrifugal acceleration of 30g. The dimensions are shown in model scale in Fig. 1. The ground model dimensions were 1000 × 450 × 300 mm. Toyoura sand (G_s = 2.64, e_{max} = 0.982, e_{min} = 0.604) was used as the test soil. The dry sand model consisted of single-layer with a nominal relative density (Dr) of 70%. The saturated sand model consisted of an upper layer with a nominal Dr of 70% (300 mm thickness) and a lower layer with a nominal Dr of 90% (150 mm thickness). The soil in the liquefiable sand model was saturated with silicone oil.

As shown in Fig. 1, accelerometers, strain gauges, and pore water pressure transducers were installed in the soil-pile-structure systems. Bending strain was measured in the black piles (A to D) with eight gauges and gray piles with two gauges (Fig. 1). Each pile contained a stainless steel pipe of 450 mm in length, 15.9 mm in diameter (D), 0.3 mm in thickness, and flexural rigidity of 9.3×10^{-2} kNm^2. The pile heads were fixed to a foundation with a pile spacing of 2.5D and the piles tips were connected to a laminar shear box using a pin connection. A superstructure of the stainless steel had a primary natural period of 0.3 s in the prototype scale. Fig. 2 shows the horizontal acceleration time histories of shaking table experiment #AG11 in both the dry sand and saturated sand models. Fig. 3 shows the time histories of excess pore water pressure in the upper part of medium sand layer (PW1) and upper part of medium to dense sand layer (PW7). The excess pore water pressure reaches its initial effective vertical pressure in both PW1 and PW7 (Fig. 3). The relative density of the upper part of medium to dense sand layer at nominal Dr of 90% may therefore have been lower than expected.

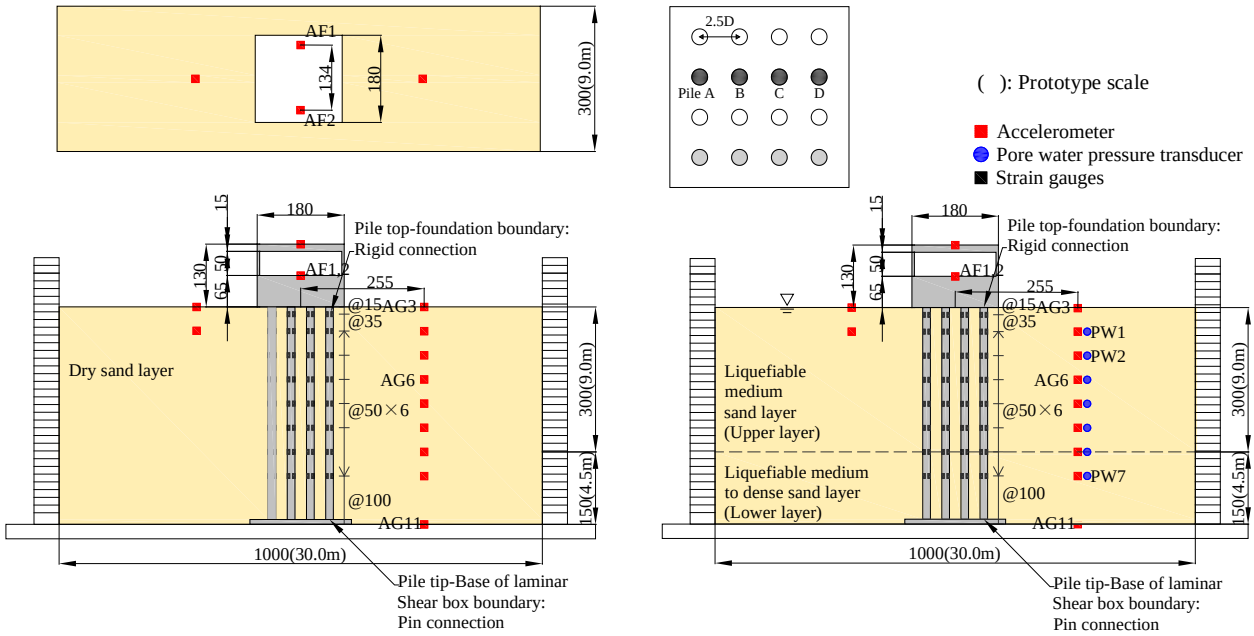

(a) Dry sand model (b) Saturated sand model

Fig. 1 – Soil-pile-structure systems (unit: mm, model scale)

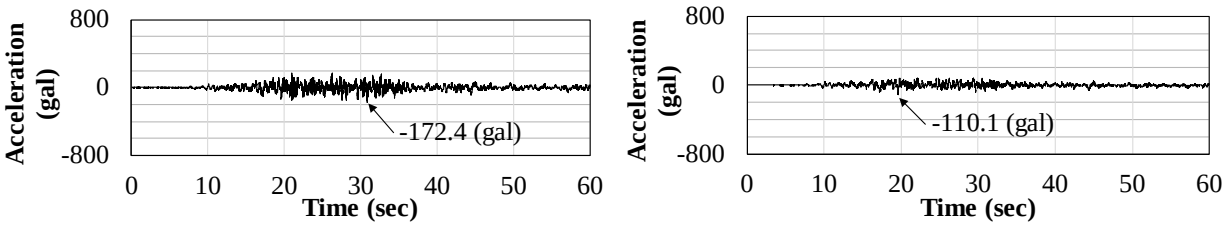

(a) Dry sand model (b) Saturated sand model

Fig. 2 – Time histories of horizontal acceleration of shaking table experiments

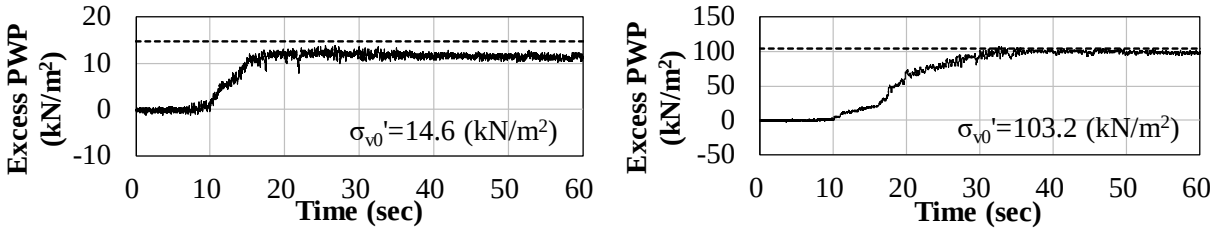

(a) PW1 (b) PW7

Fig. 3 – Time histories of excess pore water pressures in saturated sand model

3. Numerical analysis of centrifuge model test

3.1 Numerical methods

We used FLIP3D Version 1.6, which incorporates a multi-shear spring model [7], as a 3D dynamic effective stress analysis program to determine the constitutive soil behavior. The resulting matrix was solved using a parallel direct solver [8].

Fig. 4 shows the 3D finite element method (FEM) model of the saturated soil as a representative example of the analysis model. The dimensions are shown in the prototype scale and analysis conditions and results are hereafter also shown in the prototype scale. Owing to the pile group symmetry, only half of the soil-pile system was modeled and the symmetrical plane was fixed in the *y*-direction. The model bottom was completely fixed. A laminar shear box was modeled using beam elements of the same rigidity and mass as a laminar shear box composed of aluminum. Soils were modeled as in the multi-shear spring model with piles and superstructure as linear shell elements and the foundation as eight-node brick elements. The mesh division was refined around the pile periphery to ensure accuracy and coarsened away from pile periphery to reduce calculation cost. The mesh in the circumferential direction of each pile were divided into 16 parts.

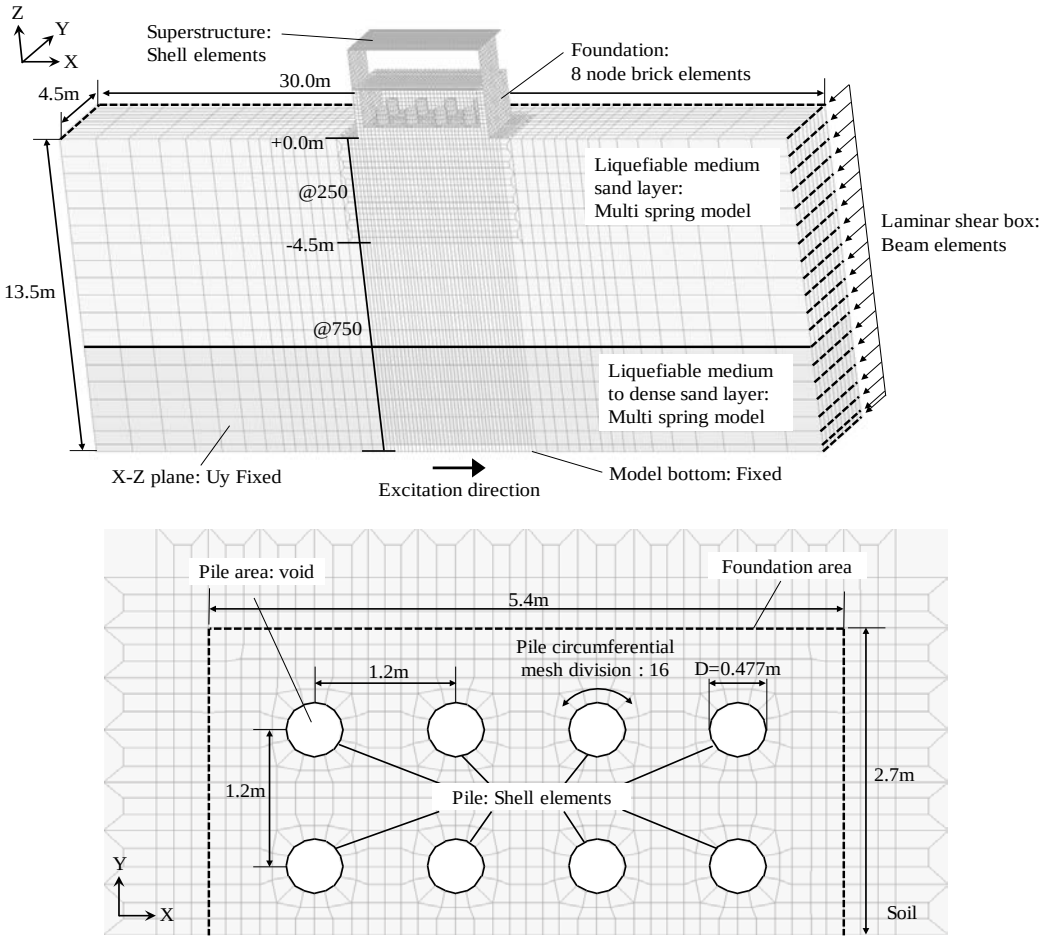

Fig. 4 – 3D finite element model of the saturated sand model

Fig. 5 details the numerical model near the piles. The pile heads were embedded in the foundation bottom and the contact surface between piles and foundation was rigidly fixed. The contact surface was free between the foundation bottom and soil surface. The contact surface between the pile surface and soil around the pile was rigidly connected both horizontally and vertically, and slip and separation were not considered. At the pile tip, the contact points between the two ends in the *y*-direction on the pile surface and the contact point with laminar shear box were rigidly connected, and the other contact points between the pile and laminar shear box were free to establish a pin connection.

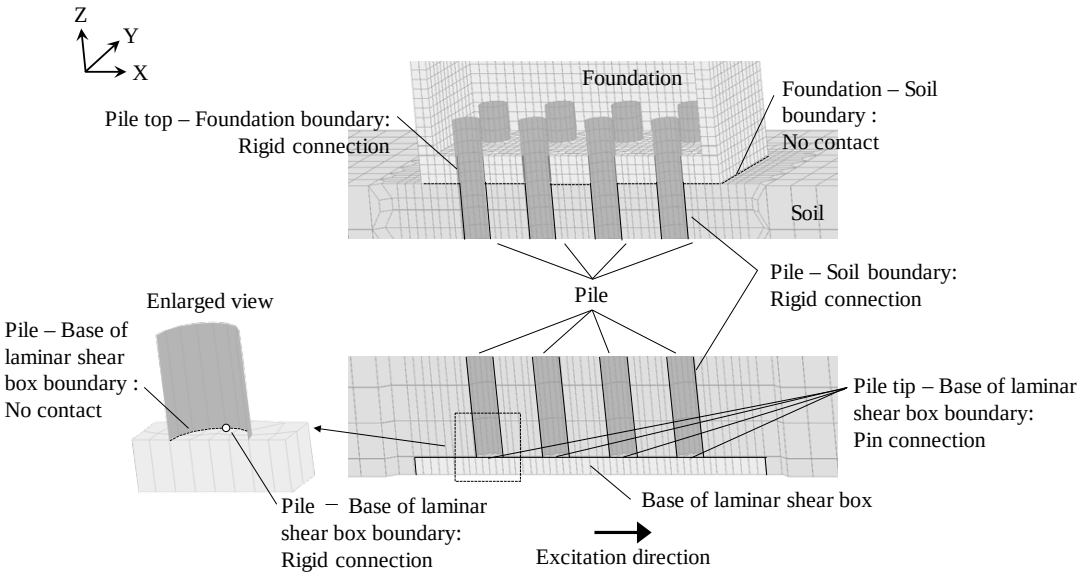

Fig. 5 – Modeling details near the piles

3.2 Dynamic deformation parameters

The soil parameters of physical and dynamic deformation characteristics used the in dry and saturated sand models are summarized in Table 1. The mass density and void ratio were based on Toyoura sand specifications and the nominal relative density given in Section 2. Silicon oil with a density of 0.955 g/cm^3 at 25 °C [9] was used to saturate the ground. The initial shear stiffness was obtained from the empirical formula of the small strain modulus of Toyoura sand expressed by porosity and initial confining pressure [10]. The shear resistance angle of soils was determined from an equation expressed by porosity and minimum porosity proposed by Caquot and Kerizel [11]. The maximum soil damping ratio was estimated from typical free-field stress-strain histories in the dry sand model assuming that the soil away from the piles is unaffected by pile behavior.

Fig. 6a shows a typical stress-strain history. The soil shear strain was calculated by numerically differentiating the displacement obtained by integrating the acceleration twice, and the shear stress determined by integrating the inertial force of the soil in the depth direction. Fig. 6b shows the relation between equivalent hysteresis damping and shear strain obtained from four cycles. A dashed line shows the HD model curve obtained from the test results. The maximum soil damping ratio estimated using this approach is 0.28.

Table 1 – Parameters of soil physical and dynamic deformation characteristics

Layer	**ρ** (t/m^3)	**n**	**G_{ma}** (kPa)	**$-\sigma_{ma}$'** (kPa)	**ϕ_f** (deg)	**ν**	**h_{max}**	**ϕ_p** (deg)
Dry sand layer	1.57	0.407	59600	29.4	40.8	0.33	0.28	—
Liquefiable medium sand layer (Upper layer)	1.95	0.407	59600	29.4	40.8	0.33	0.28	28.0
Liquefiable medium to dense sand layer (Lower layer)	2.00	0.377	110300	74.3	44.3	0.33	0.28	28.0

ρ: density; n: void ratio; G_{ma}: elastic shear modulus at a confining pressure of ($-\sigma_{ma}$'); $-\sigma_{ma}$': reference confining pressure; φ_f: shear resistance angle, $\sigma_{ma}' = \sigma_v'(1 + 2K_0)/3$, K_0: coefficient of earth pressure at rest (0.5), σ_v': effective vertical pressure at the center depth of the soil unit., **ν**: Poisson's ratio, h_{max}: maximum damping ratio

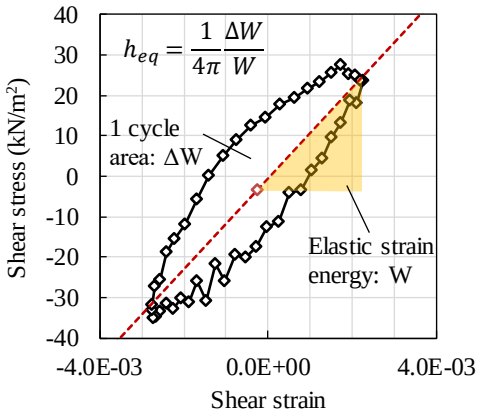

(a) Typical stress-strain history

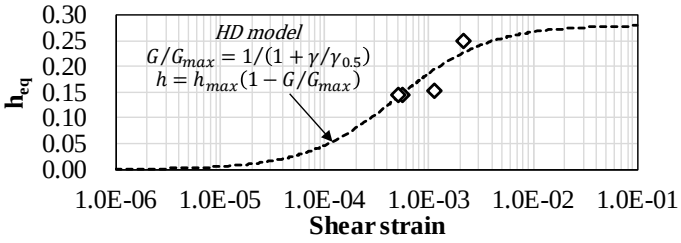

(b) Equivalent hysteresis damping (h_{eq}) - shear strain relation

Fig. 6 – Maximum soil damping ratio estimation

3.3 Liquefaction parameters

As shown in Fig. 3, the excess pore water pressure in the upper layer and upper part of the lower layer reach an initial effective vertical pressure of the corresponding test depths. Both the upper and lower layers are therefore considered liquefiable layers. Six parameters are used to define the liquefaction characteristics: phase transformation angle (φ_p); parameter controlling in the initial phase (p_1) and final phase (p_2); overall dilatancy (w_1); ultimate limit (S_1); and dilatancy threshold limit (c_1). Of these, φ_p, S_1, p_1, and p_2 were set from simplified methods to determine the FLIP parameter [12], and w_1 and c_1 were determined from cyclic shear simulations targeting the liquefaction strength obtained from laboratory tests.

The liquefaction characteristics of the upper layer (Dr = 70%) and lower layer (Dr = 90%) were based on the hollow cylinder cyclic torsional shear test using Toyoura sand (Dr = 70%) under a confining pressure of 50 kPa [13]. From the previous test, the cyclic shear strength ratio to 20 cycles (RL_{20}), in which the double amplitude of linear strain (DA) was 5%, was 0.220. The liquefaction characteristic of the upper layer (Dr = 70%) was set to an RL_{20} of 0.220. According to previous tests [14], the RL_{20} of Dr = 90% is presumed to be 1.96 times that of RL_{20} of Dr = 70%. Accordingly, the liquefaction characteristics of Dr = 90% was set to an RL_{20} of 0.431 (parameter set A in Table 2). The case of RL_{20} = 0.220 for the lower layer was also considered because of the possibility that the relative density of the lower layer may have been lower than expected, as described in Section 2 (parameter set B in Table 2). Fig. 7 shows the reproduced liquefaction resistance curves obtained by the cyclic shear simulations, and Table 2 summarizes the liquefaction parameters corresponding to each curve in Fig. 7.

Fig. 8 shows the time histories of excess pore water of PW7 obtained from trial numerical analysis using liquefaction parameters listed in Table 2. The time histories of excess pore water pressure using parameter set B agree relatively well with the experimental results, whereas those of parameter set A show little increase and differing trends from the experiments. Parameter set B was therefore used as the liquefaction characteristics of the entire lower layer.

Table 2 – Model parameters for liquefaction characteristics

Layer	ϕ_p (deg)	S_1	w_1	p_1	p_2	c_1	RL_{20}
Upper layer	28.0	0.005	2.24	0.70	0.80	2.01	0.220
Lower layer (Parameter set A)	28.0	0.005	7.40	0.50	1.00	4.01	0.431
Lower layer (Parameter set B)	28.0	0.005	1.38	0.70	0.80	1.93	0.220

φ_p: phase transformation angle, parameter control; p_1: initial phase, p_2: final phase, w_1: overall of dilatancy, S_1: ultimate limit, c_1: threshold limit of dilatancy.

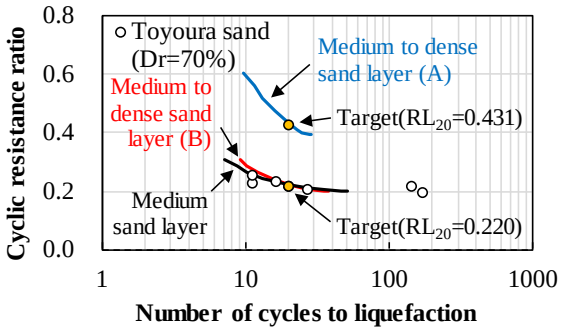

Fig. 7 – Reproduced liquefaction resistance curves

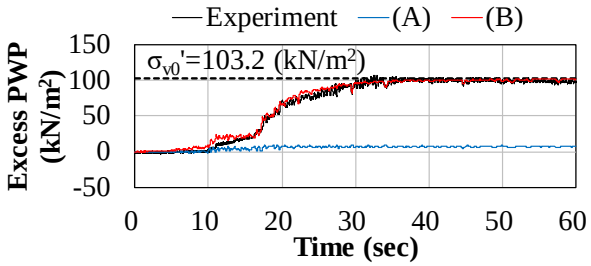

Fig. 8 – Time histories of excess pore water pressure in saturated ground (PW7)

3.4 Parameters for pile foundation and superstructure

Table 3 lists the parameters used for analysis of the piles, foundation, and superstructure. The piles consisted of a stainless steel pipe, the foundation of aluminum, and the superstructure of stainless steel. The specifications of aluminum and stainless steel were obtained from the Mechanical Engineering Handbook [15].

Table 3 – Pile foundation and superstructure specifications

Item	Material	E (kPa)	ν	ρ (g/cm^3)	h (%)
Pile	Strainless pipe	2.10×10^8	0.30	7.8	2.0
Foundation	Aluminum	7.45×10^7	0.32	2.7	2.0
Superstructure	Strainless	2.10×10^8	0.30	7.8	2.0

E: Young's modulus, **ν**: Poisson's ratio, **ρ**: density, h: initial damping ratio

3.5 Damping characteristics

The input wave had a duration of 60 s, a time step of 0.01 s, and was excited in one horizontal direction. Acceleration on the shaking table (Fig. 2) was input from the bottom of the numerical analysis model. The Wilson θ method (θ = 1.4) was used for time integration. The rigidity proportional damping was used for soil-

foundation-structure system. The rigidity proportional damping of soils was estimated from the initial natural period of free-field ground assuming an initial damping ratio of 1%. The rigidity proportional damping of the foundation and structure was estimated from the initial natural period of the structure (T_G = 0.300 s) assuming an initial damping ratio of 2%.

4. Results

4.1 Dynamic responses

Fig. 9 shows the acceleration time histories of the ground surface, underground, and top of the foundation in dry and saturated sand models. Fig. 10 shows the time histories of excess pore water pressures in the saturated sand model. Calculated accelerations of the ground surface and underground show good consistency with the measured accelerations (Figs. 9a(i), 9a(ii)). The calculated acceleration at the top of the foundation is smaller than the measured acceleration during the large excitation period (~25–35 s), but general agreement between experiment and simulation is shown before and after that period (Fig. 9a(iii)). Spike-like peaks are observed after 17 s when the excess pore water pressure increases by more than half in the experiments (Fig. 9b(i)–9b(iii)). Although these peaks are not completely reproduced in the simulation, the responses are generally consistent with experiments before the excess pore water pressure increases by more than half and after liquefaction.

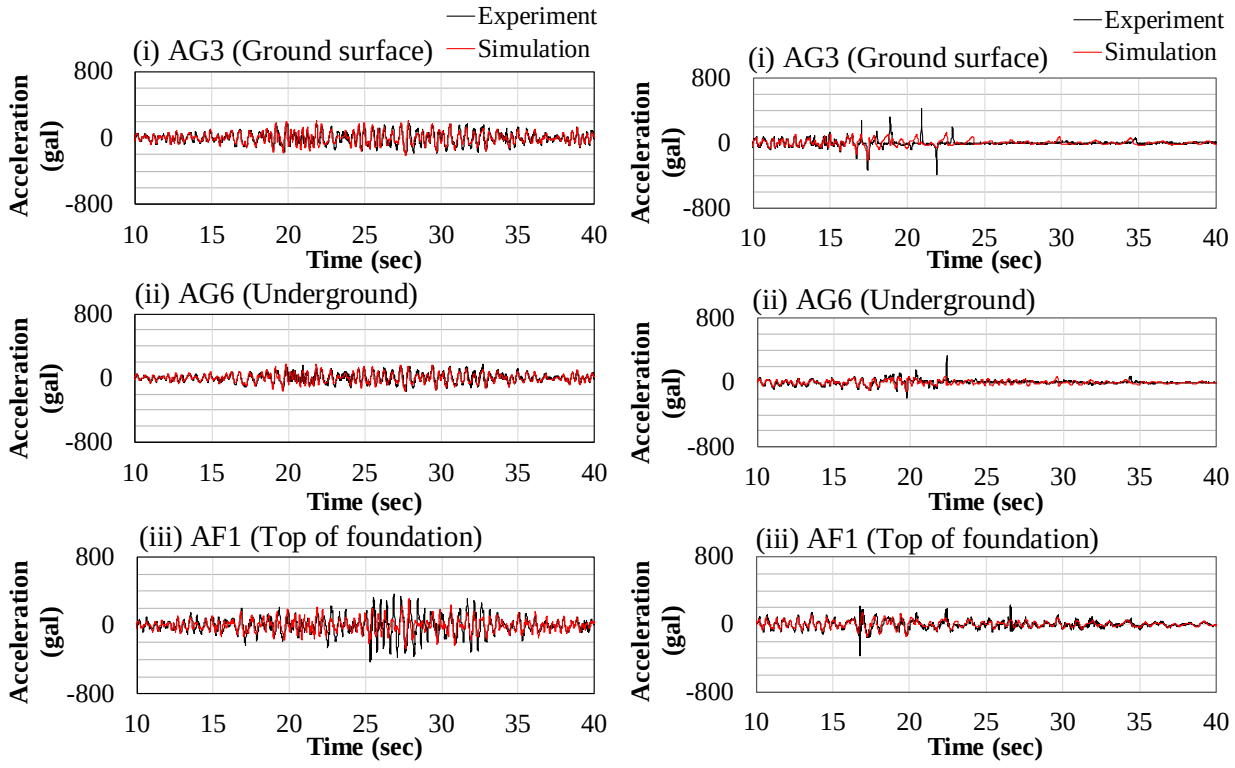

(a) Dry sand model (b) Saturated sand model

Fig. 9 – Acceleration time histories

Fig. 11 shows the time histories of bending strain at the pile heads of models A, B, and D. Although slightly smaller than measured values during the large excitation period in the dry sand model (Fig. 11a), the calculated bending strains generally reproduce the measured bending strains at the pile heads.

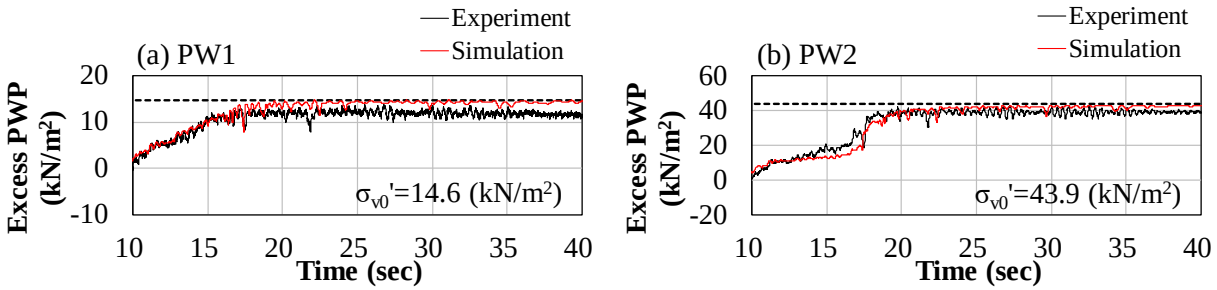

Fig. 10 – Time histories of excess pore water pressures in the saturated sand model

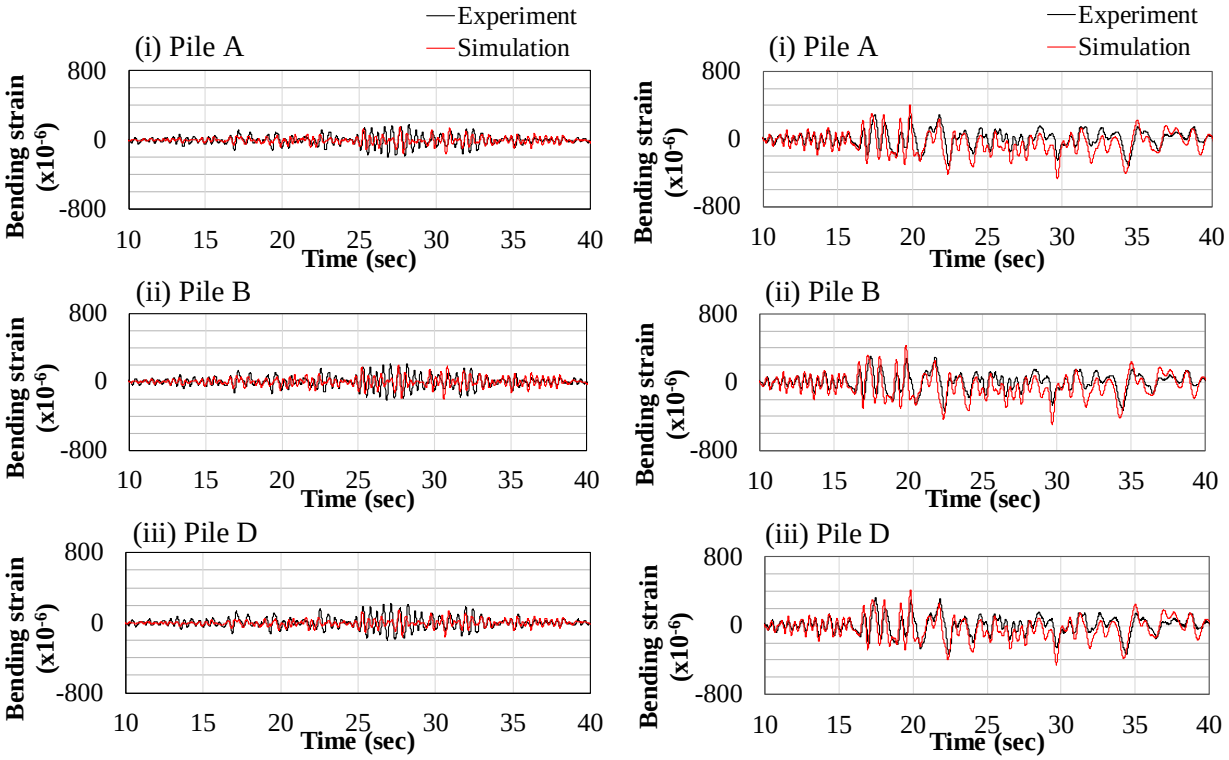

(a) Dry sand model (b) Saturated sand model

Fig. 11 – Time histories of bending strains at the pile heads of piles A, B, and D

4.2 Pile foundation behavior

Because the pile does not plasticize in the experiments, the pile bending moments are calculated from the bending strain of the planar element, a flexural rigidity of 9.3×10^{-2} kNm^2, and shear forces from differentiation of the bending moment in the depth direction. Fig. 12 shows the time histories of the bending moments at the pile heads of pile A and typical times of their depth distribution. The first letter of the typical times is an index of time, the second letter indicates experiment (E) or simulation (S), and the third character indicates the time zone. The times at which the experiments reach their maximum bending moment (t_{E0}, t_{E2}) are consistent with positive peak times from the simulations (t_{S0}, t_{S2}). Times prior to liquefaction were also selected in the saturated sand model (t_{E1}, t_{S1}). Figs. 13 and 14 show the results of the dry and saturated sand models, respectively, for the bending moment depth distributions of piles A to D. The peak depth of the bending moment tends to be slightly higher in the simulations compared with the experiments, but the peak

amplitude is generally consistent in dry sand model (Fig. 13) and the depth distributions of the simulations are in generally good agreement before and after liquefaction in the saturated sand model (Fig. 14).

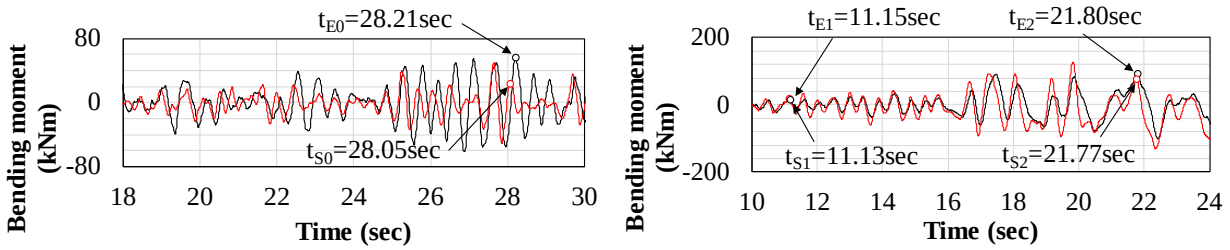

(a) Dry sand model (b) Saturated sand model

Fig. 12 – Time histories of bending moments at the pile head of pile A

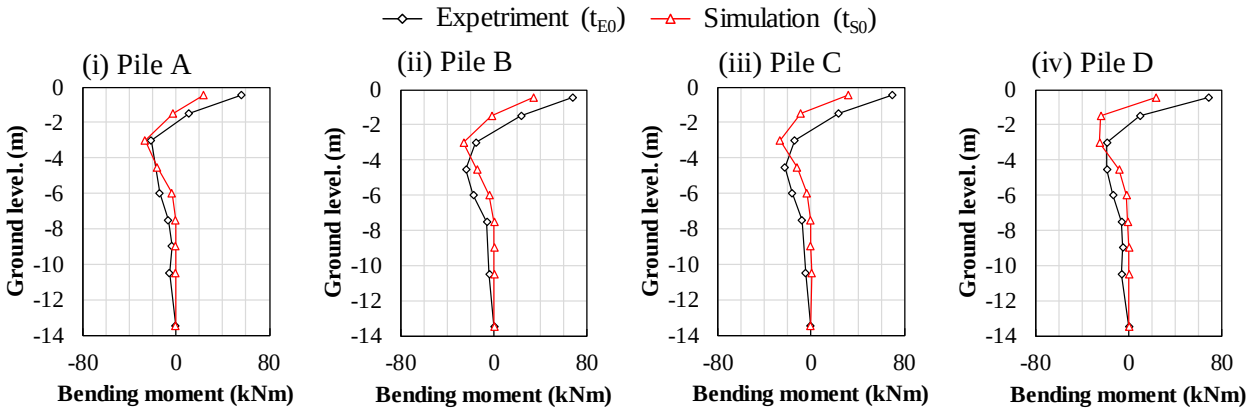

Fig. 13 – Depth distribution of bending moments in the dry sand model

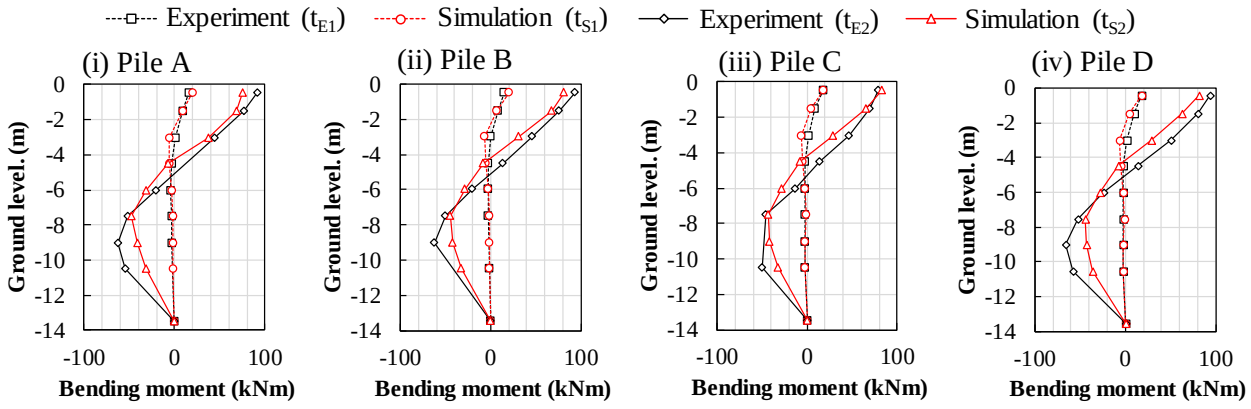

Fig. 14 – Depth distribution of bending moments in the saturated sand model

Figs. 15 and 16 show the results of the dry sand and saturated sand models for the depth distributions of shear forces of pile A to D. Fig. 17 shows the plane distributions of shear forces at pile heads of both models. The times shown in Figs. 15–17 are t_{E0} and t_{S0} in the dry sand model and t_{E2} and t_{S2} in the saturated sand model. The peak depth of shear forces tends to be slightly higher in the simulations, but the peak amplitudes are generally consistent with the experiments (Figs. 15, 16). The experiments and simulations both show larger

shear forces at the pile heads of the dry sand model (Fig. 17a) compared with the saturated sand model (Fig. 17b). Calculated shear forces of the dry sand model tend to be larger in the leading pile compared with the trailing pile, which matches the experimental results (Fig. 17a), whereas this difference is smaller in the saturated sand model, which is also verified by the experiments (Fig. 17b).

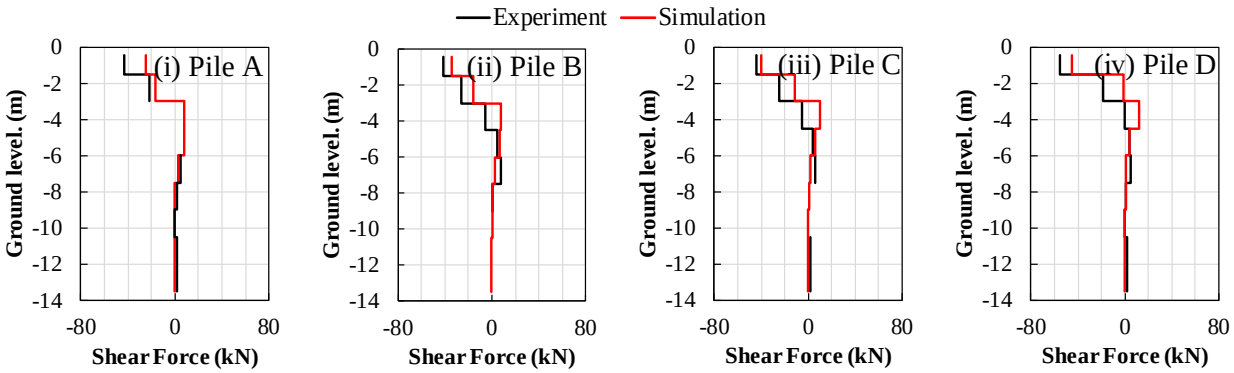

Fig. 15 – Depth distribution of shear forces in the dry sand model (experiment: t_{E0}, simulation: t_{S0})

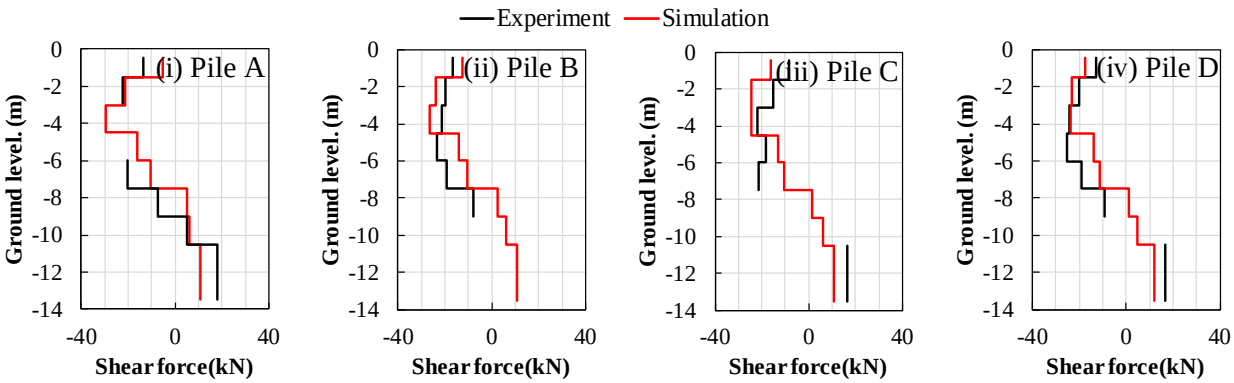

Fig. 16 – Depth distribution of shear forces in the saturated sand model (experiment: t_{E2}, simulation: t_{S2})

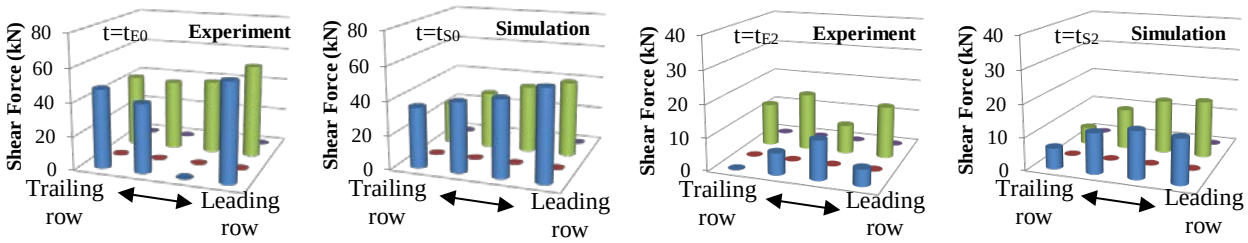

(a) Dry sand model (b) Saturated sand model

Fig. 17 – Plane distribution of shear forces at the pile heads

5. Conclusions

We conducted 3D dynamic effective stress analysis of shaking table tests of soil-foundation-structure systems under a centrifugal acceleration of 30g and examined the validity of this approach for pile foundation structures. The main conclusions are as follows.

(i) The calculated acceleration response is consistent with measured accelerations at the top of the foundation in both non-liquefied and liquefied ground.

(ii) The calculated bending moments and shear forces at pile top agree reasonably well with measured responses.

(iii) Experiments and simulations both show higher shear forces in pile heads of the dry sand model compared with the saturated sand model. Shear forces are also higher in the leading pile compared with the trailing pile, with larger differences observed in the dry sand model.

Our results indicate that a 3D FEM model with a strain-space multiple-mechanism model is applicable to studying soil-pile-structure systems in liquefied ground for the evaluation of the dynamic system behavior under horizontal motion. Differences between the experimental results and simulations under large excitations may be owing to locally loose soil around the pile during model development. This implies the necessity to further study the method of ground modeling around the piles.

6. References

[1] Iai S (2018): *Developments in Earthquake Geotechnics.* Springer International Publishing.

[2] Tamari Y, Ozutsumi O, Ichii K, and Iai S (2018): Simplified method for nonlinear soil-pile interactions in two dimensional effective stress analysis. *Geotechnical Earthquake Engineering and Soil Dynamics Conference V, Numerical Modeling and Soil Structure Interaction*, 258-268, Austin, USA.

[3] Cheng Z, Jemeric B (2009): Numerical modeling and simulation of pile in liquefiable soil. *Soil Dynamics and Earthquake Engineering*, **29** (11-12), 1405-1416.

[4] Jimenez GAL, Dias D, Jeneck O (2019): Effect of layered liquefiable deposits on the seismic response of soil-foundations-structure systems. *Soil Dynamics and Earthquake Engineering*, **124**, 1-15.

[5] Su L, Wan HP, Li Y, Ling XZ (2018): Soil-pile-quay wall system with liquefaction-induced lateral spreading: experimental investigation, numerical simulation, and global sensitivity analysis. *Journal of Geotechnical and Geoenvironmental Engineering*, **144** (11), 04018087.

[6] Suzuki H, Tokimatsu K, Ozawa G (2006): Estimation of group pile effects in non-liquefied and liquefied ground based on centrifuge model tests. *Proceedings of the 8th US National Conference on Earthquake Engineering*, San Francisco, USA.

[7] Iai S (1993): Three dimensional formulation and objectivity of a strain space multiple mechanism model for sand. *Soils and Foundations*, **33** (1), 192-199.

[8] Amestoym PR, Duff IS, L'Excellent JY (2000): Multifrontal parallel distributed symmetric and unsymmetric solvers. *Computer Methods in Applied Mechanics and Engineering*, **184** (2-4), 501-520.

[9] Shin-Etsu Silicone (2003): Performance test results of silicon oil KF-96. (https://www.silicone.jp/catalog/pdf/kf96_j.pdf)

[10] Ishihara K (1996): *Soil Behaviour in Earthquake Geotechnics*. Oxford University Press.

[11] Moroto N (1983): Angles of internal friction for sand and gravel. *Soil Mechanics and Foundation Engineering*, **31** (8), 5-10. [in Japanese]

[12] Morita T, Iai S, Liu H, Ichii K, Sato Y (1997): Simplified method to determine parameter of FLIP. *Technical Note of the Port and Harbour Research Institute*, **869**. [in Japanese]

[13] Tanaka T, Yasuda S, Naoi K (2009): Liquefaction of various quartz sand under low confining pressure and deformation behavior after liquefaction. *Journal of the 30th JSCE Earthquake Engineering Symposium*, 2-0013. [in Japanese]

[14] E-Defense (2005): Physical properties test of soil in large tank experiments (http://www.bosai.go.jp/hyogo/ddt-pj/report/result17/3.3/3.3.2.pdf)

[15] Japan Society of Mechanical Engineering (JMSE) (1985): *JMSE Mechanical Engineer's Handbook*, B4.

